Coastal Engineering 140 (2018) 292–305

Contents lists available at ScienceDirect

Coastal Engineering

journal homepage: www.elsevier.com/locate/coastaleng

Extreme coastal responses using focused wave groups: Overtopping and horizontal forces exerted on an inclined seawall

C.N. Whittaker[a,*], C.J. Fitzgerald[e], A.C. Raby[b], P.H. Taylor[c], A.G.L. Borthwick[d]

[a] Department of Civil and Environmental Engineering, Faculty of Engineering, University of Auckland, Symonds St, Auckland, 1010, New Zealand
[b] Department of Marine Science and Engineering, Faculty of Science and Engineering, Plymouth University, Drake Circus, PL4 8AA, UK
[c] Department of Engineering Science, University of Oxford, Parks Rd, Oxford, OX1 3PJ, UK
[d] School of Engineering, The University of Edinburgh, The King's Buildings, Edinburgh, EH9 3JL, UK
[e] Inland Fisheries Ireland, 3044 Lake Drive, Citywest Business Campus, Dublin, D24 Y265, Ireland

ARTICLE INFO

Keywords:
Overtopping
Seawall
Forces
Focused wave groups
Wave-maker theory
Spurious error wave
Boussinesq numerical wave tank
Extreme waves

ABSTRACT

Total wave group overtopping and maximum horizontal force responses are investigated for an idealised seawall/dike on a plane beach subject to compact focused wave attack, using both laboratory and numerical wave flumes. The wave group interactions have very short durations such that extraneous reflections from the wavemaker arrive long after the main interaction. These short test durations facilitate the use of large ensembles of tests to explore the sensitivity of overtopping and force responses to variations in focus location, phase angle at focus, and linear focus wave amplitude. The scope of the laboratory wave flume tests is broadened by accurate numerical simulation based on a 1DH hybrid Boussinesq-NLSW model.

For a given focus location and linear focused wave amplitude, variations in phase lead to an order-of-magnitude change in the group overtopping volume. Substantial increases in overtopping volume owing to the use of linear wavemaker theory (compared to second order theory) are also observed. These observations have implications for phase-independent empirical relationships derived using linear paddle signals in physical experiments. Examination of the incidence of wave groups parametrically optimised for maximum (and minimum) overtopping volumes indicates that the overtopping volume may be optimised by minimising reflections of pre-overtopping waves within the group, while maximising the amplitude of the first overtopping bore. Numerical predictions of horizontal seawall forces are obtained using fluid impulse derivatives and hydrostatic pressures obtained from the shallow water model. Within the shallow water model framework, hydrodynamic force contributions included in the fluid impulse method are observed to be small relative to the hydrostatic pressure force. The parametric dependence of the horizontal (non-impulsive) forces on the seawall is very similar to that of the overtopping volumes, with clear 'bands' of large values observed as a function of phase and focus location (for a given amplitude). This suggests that the parametric optimisation of focused wave groups is a robust method for the investigation of multiple coastal responses such as overtopping, forces and runup.

1. Introduction

Extreme overtopping of coastal defence structures during a storm leads to coastal flood inundation which may cause significant economic damage and threaten life in vulnerable coastal communities, particularly where residents are unaware of the risks posed by overtopping (Allsop et al., 2003; Hughes and Nadal, 2009). As such, the reduction of overtopping risk is a key design requirement for seawalls and other coastal structures (Van der Meer et al., 2016; Pullen et al., 2007; Van der Meer, 1998). 'Green water' overtopping occurs where waves running up the face of a coastal structure exceed the crest level of the structure, such that a continuous sheet of water passes over the crest, and is the strongest contributor to overtopped volumes (Van der Meer et al., 2016; Ingram et al., 2009; Goda, 2009; Hughes and Nadal, 2009). Changes in forcing by rising sea levels and increased storminess, coupled with ageing flood protection infrastructure, imply that wave overtopping of coastal structures will increase in importance in the future (Geeraerts et al., 2007).

Design guidance for the prediction of wave overtopping is given in the EurOtop Manual on Wave Overtopping of Sea Defences and Related Structures (Pullen et al., 2007), which has recently been enhanced (Van der Meer et al., 2016). These manuals have been developed from large

* Corresponding author.
E-mail address: c.whittaker@auckland.ac.nz (C.N. Whittaker).

https://doi.org/10.1016/j.coastaleng.2018.08.004
Received 28 March 2018; Received in revised form 21 July 2018; Accepted 2 August 2018
Available online 13 August 2018

databases of physical model studies, numerical simulations, and available field data. The present paper discusses the results of small-scale physical experiments (with accompanying numerical simulations) on overtopping and forces exerted on an idealised seawall. Our results demonstrate the importance of the method of wave generation on overtopping measurements, and on design standards (which rely on databases of such measurements). Focused wave groups provide insight into the relationship between incident wave properties and coastal responses (such as overtopping and forces), and may provide a complementary design approach for coastal structures subject to wave loading.

Field measurements of average overtopping rates gathered at the Zeebrugge rubble-mound breakwater from 1999 to 2003 by Troch et al. (2004) provided a robust dataset for validation of the empirical formulae presented by van der Meer et al. (1998) and Owen (1982). Additional field data were obtained from the Rome yacht harbour rubble-mound breakwater in Ostia, Italy (Briganti et al., 2005) and Samphire Hoe, United Kingdom (Pullen et al., 2009). Significant differences in overtopping volume measured in two- and three-dimensional laboratory replication of two sets of storm observations from the Ostia site (Franco et al., 2009) were attributed to scale effects (particularly those relating to wave breaking processes). The hydrodynamics of flows overtopping dikes, and the damage caused by these flows, have been investigated in detail using an overtopping simulator (e.g. van der Meer et al., 2011). Altomare et al. (2016) demonstrate the necessity to include the effect of very shallow foreshores on the predicted average overtopping discharge over dikes; see Chen et al. (2016) for a discussion of these effects on impacts on a vertical wall constructed on a dike crest (Chen et al., 2015; Van Doorslaer et al., 2017).

The European research project CLASH (Crest Level Assessment of coastal Structures by full scale monitoring, neural network prediction and Hazard analysis on permissible wave overtopping), discussed by Geeraerts et al. (2007), included the collation of experimental results from approximately 10,000 irregular wave overtopping tests (van der Meer et al., 2009) for the purpose of deriving empirical formulae and training a neural network (NN) prediction method (see van Gent et al., 2007; Verhaeghe et al., 2008; Lykke Andersen and Burcharth, 2009; Zanuttigh et al., 2016; Pillai et al., 2017).

Bruce et al. (2009) included the effect of surface roughnesses of different armour types on average overtopping discharge and wave-by-wave overtopping volumes within the database (see also Molines and Medina, 2015). Hughes and Thornton (2016) highlighted the need to account for the properties of individual overtopping waves, and obtained individual overtopping discharge as the product of flow thickness and horizontal velocity of the flow overtopping a dike (see also Hunt-Raby et al., 2011). van Damme (2016) derived distributions for overtopping wave properties based on runup parameters, arguing that these are more appropriate than empirically-derived overtopping parameters; this paper uses focused wave groups for the same reason.

Much of the numerical modelling of wave overtopping has been undertaken based on either the nonlinear shallow-water (NLSW) equations (e.g. Hubbard and Dodd, 2002; Tuan and Oumeraci, 2010; Williams et al., 2014), or a hybrid model that couples the NLSW equations with the Boussinesq equations, the latter to include the effects of dispersion (Orszaghova et al., 2012, 2014; McCabe et al., 2013; Tonelli and Petti, 2013). Numerical studies have also used volume of fluid (VOF) solvers to capture the complexity of overtopping and related coastal processes (Li et al., 2004; Losada et al., 2008; Reeve et al., 2008; Ingram et al., 2009; Higuera et al., 2013, 2014a, 2014b; Jacobsen et al., 2015; Vanneste and Troch, 2015; Tofany et al., 2016; Castellino et al., 2018). Smoothed particle hydrodynamics (SPH) models are often applied to these problems for the same reason (Gomez-Gesteira et al., 2005; Dalrymple and Rogers, 2006; Akbari, 2017). Numerical modelling often requires a compromise between the desire to capture correctly the complex physics of runup processes at the coast and the need for a sufficient number of simulations to obtain robust statistical distributions of the parameters of interest (motivating studies using more computationally efficient models such as SWASH by Suzuki et al., 2017).

Wave impact forces on vertical and sloping coastal structures are highly variable, and have been studied in wave flume experiments over a range of scales. Oumeraci et al. (1993) provide a qualitative description of the wave breaking processes affecting impact forces on a caisson (Neelamani et al., 1999, also found that maximum pressures on an impermeable seawall increased with Iribarren number), and the influence of caisson geometry on these impact forces. Oumeraci et al. (2001) suggested a predictive method for quasi-static and impulsive wave loadings based on a series of tests undertaken in a large wave flume within the framework of the PROVERBS project (Allsop et al., 1996). Cuomo et al. (2010) investigated scale effects on the impulsive and quasi-static loads on a vertical seawall. Chen et al. (2015) investigated the forces exerted on a vertical wall located on a dike crest, including the effect of a shallow foreshore (Chen et al., 2016). Orszaghova et al. (2014) demonstrated that the results of several of these studies may be affected by the error wave generated by a first-order wave maker signal.

The question arises: can we obtain statistically meaningful results from short-duration tests, i.e. shorter than the standard recommended length of 1000 irregular waves? Romano et al. (2015) concluded from their sensitivity analysis that the record length may be reduced to 500 waves without a loss of accuracy. Building on this work, can isolated large wave overtopping or force events be related more directly to the extremes within a given sea state? A design approach involving short-duration focused wave group model tests could complement existing long-duration irregular wave methods yielding potential benefits such as: increased repeatability, assessment of model effect and the possibility of enhanced measurement resolution for the large wave interactions. Consequently, detailed examinations of conditions leading to large responses would be possible.

In offshore engineering, Tromans et al. (1991) introduced a compact focused wave group referred to as NewWave for design purposes (see Whittaker et al., 2017, for a detailed description of this design wave in a coastal context). NewWave theory relates the expected shape of a large wave in a (linear) sea state to the bulk properties of the sea state, based on the rigorous statistical analysis of extremes for linear, Gaussian processes by Lindgren (1970). Where survivability of structures subject to extreme events plays a significant role in design, the NewWave approach provides an attractive alternative to either long irregular wave or regular wave design methods. In particular, an extreme response within a specified period of irregular wave incidence could be accurately reproduced with a short duration test (Jonathan and Taylor, 1997).

NewWave focused wave groups are increasingly being studied in a coastal engineering context, e.g. in examining runup and flow kinematics at plane beaches (Borthwick et al., 2006; Whittaker et al., 2017), and are being utilised as tools in coastal response investigations, e.g. physical experiments on wave overtopping of seawalls by Hunt (2003); Hunt-Raby et al. (2011); Hofland et al. (2014). Whittaker et al. (2016) have recently demonstrated the validity of NewWave as a model for pre-breaking waves in relatively shallow-water conditions, suggesting that extreme coastal responses within a given sea state might be reproduced using a single extreme incident wave group. Following similar reasoning, the 'NewForce' model has been recently proposed to capture the shapes of extreme wave forces on monopiles, Schløer et al. (2017). Therefore, a clear scope exists for possible application of this NewWave design approach within coastal design procedures.

In this paper, we examine the overtopping responses and non-impulsive or pulsating wave loads on an idealised gently sloped seawall (or dike) situated on a plane beach, subject to incident NewWave-type focused wave groups. Response sensitivity to the (linear) focused wave group envelope amplitude, linear focus location, and phase angle of the

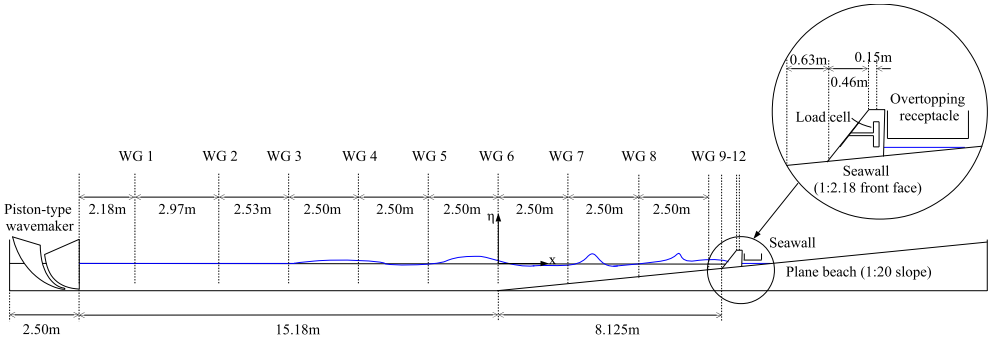

Fig. 1. Experimental setup used in overtopping and force tests at the COAST Laboratory, Plymouth University (UK). Wave gauges are represented by the abbreviation WG.

wave group at focus are examined. Parametric optimisation[1] is achieved by varying the focus location and phase at focus for a given wave group envelope amplitude. That is, the same energy is propagated through the flume, but where and how the waves focus are varied. Typically, maximum overtopping occurs for focus locations in the vicinity of the seawall. However, a large variation in overtopping volume is observed depending on the phase of the waves at focus (e.g. as a crest or trough) for prescribed incident wave energy. The variability in wave overtopping results as a function of seeding number (i.e. wave phasing) has been investigated in numerical studies by McCabe et al. (2013) and Williams et al. (2014) and in experimental studies by Romano et al. (2015). The present study extends these results by explicitly considering the phase of a compact focused wave group.

Section 2 provides full details of the seawall and associated measurement instruments. Parametric optimisation, described in Section 3, is conducted using both physical and numerical wave flumes. Section 4 presents an overview of the OXBOU model (Orszaghova et al., 2012) and a validation case study from the present set of laboratory tests. Section 5 provides comparisons of the experimental measurements and numerical predictions of total overtopping volumes for each wave group. A comparison of numerically predicted maximum individual and group overtopping volumes is presented in Section 5.3. We also seek to extract horizontal wave load information from the numerical model output, and compare the results with laboratory measurements of the horizontal load cell installed in the model seawall. Section 6 compares the numerical prediction with experimental measurement of the maximum horizontal (non-impulsive) forces on the seawall.

2. Experimental method

2.1. Physical laboratory setup

The physical experiments were conducted in a wave flume of 35 m length, 0.6 m width, and 0.5 m still water depth at the wavemaker, located in the COAST (Coastal, Ocean and Sediment Transport) Laboratory, Plymouth University (UK). Fig. 1 shows the experimental setup. A model seawall with a 1: 2.18 (vertical:horizontal) front face and horizontal seawall crest length of 0.3 m was constructed on a 1: 20 plane beach, with the beach toe 15.17 m from the wavemaker and the seawall toe 8.125 m horizontally from the beach toe, giving a local still water depth of 0.09375 m at the seawall toe and a freeboard of 0.117 m at the flat top of the seawall. The seawall and beach geometry follows that used in the wave basin experiments of Hunt-Raby et al. (2011), although the distance between the wavemaker and the beach toe was different. The beach was constructed as a steel box section frame, overlaid with 12 mm polypropylene sheets and supported at regular intervals by stainless steel channels bolted to fixing points in the flume sidewalls. Box sections used in the frame construction ensured that the beach remained rigid under wave attack, and the polypropylene panels were fixed at their edges and centres to limit their flexure during experiments. Due to its more complicated geometry, the seawall frame comprised 15 mm acrylic webs instead of stainless steel box sections. The seawall panels were also constructed from 15 mm acrylic.

Incident waves were generated using an EDL (Edinburgh Designs Ltd.) double-element piston-type wavemaker. Focused wave groups are by definition compact, and so absorption of waves reflected by the seawall was not as important as would be the case in long-duration irregular wave tests. The wavemaker was operated under (indirect) displacement control mode only, where the paddle displacements were calculated by applying a transfer function to a target free surface elevation time series at a given location.

The use of a linear paddle signal in a physical experiment causes the generation of predominantly sum and difference frequency error waves at second order according to Schäffer (1996). Such error waves propagate from the wavemaker at different characteristic speeds, the long wave faster than the main wave group and high frequency error waves more slowly. How well separated the error waves are from the main wave group depends on the distance downstream from the paddle. Orszaghova et al. (2014) demonstrated that difference frequency waves artificially increase the runup and overtopping by focused wave groups. By implication, runup and overtopping measurements from irregular wave experiments using linear paddle signals may be overly conservative. The theory of Schäffer (1996) provides correction signals for removal of error waves for an idealised piston wavemaker, which facilitated removal of approximately 60% of the sub-harmonic error wave in the experiments of Whittaker et al. (2017). The imperfect removal of the error wave was caused by the lack of direct displacement control of the EDL wavemaker, the low-frequency limit of the wavemaker, and the difference between experimental and idealised piston wavemaker transfer functions. The partial second-order correction can be roughly approximated using an idealised piston wavemaker by eliminating the lowest difference frequency component of the signal; however, differences in the linear transfer function mean the imperfect removal of the error wave in the laboratory is only approximately reproduced. Fig. 2 displays the paddle displacement time-histories of the EDL wavemaker (partially corrected to second-order) and the idealised wavemaker with full and partial second-order correction. Hence, the overtopping volumes measured in the physical experiments are expected to be larger than the model predictions. However, the advantage of the physical experiments is that these include the full problem physics (at laboratory scales), so should provide a more accurate model of wave-structure interaction at full scale.

A low-profile load cell measured the horizontal forces exerted by the focused wave groups on the central 300 mm of the front face of the seawall from its intersection with the beach to the horizontal crest

[1] The responses of overtopping and forces are optimised in the sense that for a given wave group input with adjustable parameters it is the result when the output is maximum. However, we acknowledge that the maximum response is unlikely to be desirable from a coastal engineer's perspective (although it is what they would get for a given combination of parameters).

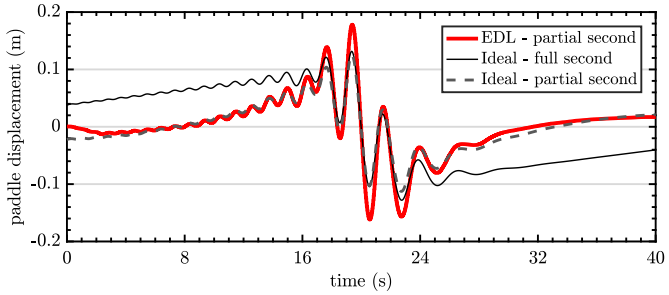

Fig. 2. Displacement time-histories for EDL piston-type wavemaker (red), ideal piston wavemaker with full second-order correction (black) and partial second-order correction (grey, dashed) for a NewWave focused wave group. (For interpretation of the references to colour in this figure legend, the reader is referred to the web version of this article.)

(referred to as the 'horizontal load cell' in the remainder of this paper). An instrumented receptacle provided measurements of the overtopped volume for the same central 300 mm section of the flume.

Free surface elevations were measured using standard resistance-type gauges along the length of the flume; several gauges were also embedded in the seawall crest to measure the elevation of the overtopping flow. Due to their relatively close spacing (0.15 m), gauges on the crest of the seawall were offset in the lateral direction to avoid interference between the gauge measurements. Moreover, the inevitable lateral variability in the breaking process, subsequent bore runup and overtopping flow caused a reduction in the repeatability of gauge measurements at the seawall crest compared to measurements further offshore (see Hofland et al., 2015, for a discussion of laboratory methods for runup and overtopping experiments).

2.2. Measurement of overtopping volumes

In this study, group overtopping was captured within an instrumented receptacle, of length 0.5 m and width 0.3 m, containing a load cell (referred to as the 'overtopping receptacle load cell' to avoid confusion with the horizontal load cell used to measure the forces exerted on the seawall). Overtopping receptacle load cell measurements at the start and end of each experiment were used to calculate the overtopped volume of the focused wave group.

2.3. Measurement of horizontal forces exerted on the front face of the seawall

Horizontal seawall forces were measured using a horizontal load cell which resisted the motion of a panel covering the central 300 mm portion of the front face of the seawall. Although the edges of this panel were sealed, after *in situ* calibration the horizontal load cell exhibited a linear response over the range of forces experienced during the experiments. The calibration, conducted in both wet and dry conditions, was achieved by hanging known masses from a pulley behind the seawall.

The seawall was wet-backed in the physical experiments, such that reflected waves from the end of the flume beyond the seawall would exert horizontal forces on the seawall. However, the wave groups tested were sufficiently compact that force signals from incident and reflected wave groups were well separated in time. The maximum (positive) horizontal force exerted on the seawall was selected for parametric optimisation because of its importance in seawall design and safety.

3. Parametric optimisation with NewWave focused wave groups

3.1. NewWave focused wave group

A focused wave group represented by linear theory comprises wave components with specified frequencies, amplitudes, and phases which coincide at a particular location and time to produce a large wave event. Where frequency dispersion is the dominant physical mechanism determining wave kinematics and dynamics, high-frequency and low-frequency components of the wave group will have very different individual velocities. Therefore, away from focus the wave group energy will be significantly dispersed, and the energy will be strongly localised, in both time and space, only around the focus event.

The NewWave focused wave group, based on a probabilistic analysis of the shape of a maximum in a linear, Gaussian process (Lindgren, 1970), describes the most probable shape of a large wave in a given sea state (Boccotti, 1983). Lindgren (1970) showed that the shape of a large event (wave) comprises both deterministic and random components, with the deterministic component dominating for events large relative to the underlying process (sea state). This deterministic component, the NewWave profile, is simply the scaled autocorrelation function, i.e. the Fourier transform of the energy density spectrum for the underlying sea state, and so the amplitude components are proportional to $S_{\eta\eta}(\omega)\cos\omega t\ \Delta\omega$ where $S_{\eta\eta}$ is the power spectral density, ω is angular frequency, and t is time. Therefore, a NewWave-type focused wave group comprising N infinitesimal wave components is given by

$$\eta(x,\ t) = \frac{A}{\sigma^2}\sum_{i=1}^{N} S_{\eta\eta}(\omega_i)\cos(k_i(x - x_f) - \omega_i(t - t_f) + \phi)\Delta\omega, \tag{1}$$

where σ is the standard deviation of the sea state (with an associated variance $\sigma^2 = \sum S_{\eta\eta}(\omega_i)\Delta\omega$ in this discretised form) and k_i is the wavenumber of the i-th wave component with angular frequency ω_i, which are related by the familiar linear dispersion relation $\omega^2 = gk\tanh kh$ (where g is the acceleration due to gravity and h is the water depth), and x is the horizontal distance. All wave components come into phase at the focus location x_f and focus time t_f to yield a large wave event with a linear focus (envelope) amplitude A. We allow the full range of focusing behaviours to occur by introducing the parameter ϕ referred to as the phase angle of the group at focus. For example, crest-focused waves correspond to a zero phase at focus $\phi = 0$ whereas trough-focused waves correspond to $\phi = \pi$.

NewWave theory was originally developed for offshore applications (Tromans et al., 1991) and first validated in deep water (Jonathan and Taylor, 1997) and thereafter in intermediate depths (e.g. Taylor and Williams, 2004; Santo et al., 2013). Recently, Whittaker et al. (2016) demonstrated that the range of validity of NewWave theory extends into shallow water by comparison with buoy data recorded during two severe storms in January 2014 at two coastal locations in the south-west of the UK, at depths h of 10 m and 15 m (with corresponding kh values of approximately 0.5). This implies that linear frequency dispersion remains the dominant mechanism driving the statistics of wave elevation outside the main breaker line despite the increasing importance of nonlinear and local bathymetric effects.

3.2. Focused wave parameter space

The effect is now examined of variations in the linear focused wave and envelope amplitude A, linear focus location x_f, and phase angle of the group at focus ϕ on total overtopping volumes and maximum horizontal bulk forces on a seawall. Table 1 lists the parameter space for the overtopping and force tests. The seawall is positioned on an impermeable plane beach of 1:20 slope, near the still water shoreline, in water of constant depth 0.5 m offshore of the beach. We consider three different linearly-focused wave amplitudes, five focus locations inshore of the beach toe, and 12 phase angles with increments of 30°. An amplitude $A = 0.057$ m was taken to be the minimum value for which substantial overtopping would occur throughout the parameter space based on preliminary laboratory tests. The magnitude of the desired second-order paddle stroke was found to exceed that possible with the particular wave paddle available for linear focus amplitudes above

Table 1
Focused wave amplitudes, focus locations and phases at focus considered for the force/overtopping laboratory tests and numerical simulations.

Parameter	Experimental values	Numerical values
A (m)	0.057, 0.0855, 0.114	0.057, 0.0855, 0.114
x_f (m) relative to beach toe	0, 5, 10, 12.5, 15	0, 2.5, 5, 7.5, 10, 12.5, 15
relative to seawall toe	−8.12, −3.12, 1.88, 4.38, 6.88	−8.12, −5.62 -3.12, −0.62, ···, 6.88
ϕ (degrees)	30, 60 …, 330, 360	15, 30, 45, …, 345, 360

0.114 m.

Focus locations were varied from the beach toe to more than 5 m beyond the seawall encompassing a total range of 15 m. The theoretical focus location controls dispersion of the wave group as it shoals and breaks during propagation up the beach slope. Intuitively, a focus location in the vicinity of the seawall (or still water shoreline) should mean the focused wave group energy arrives in a compact form at the shore leading to large coastal responses. A focus location offshore of the beach toe would allow defocusing or dispersion of the propagating wave group before it reaches the seawall. Similarly, the components of a wave group with a focus location far beyond the still water shoreline will not focus through linear superposition and the total wave group energy will arrive at the seawall in a dispersed form although shoaling effects may induce nonlinear focusing near the seawall. The range of focus locations given in Table 1 was considered to be sufficiently wide to capture the most extreme responses.

The phase angle at focus ϕ provides a means to control the nature of the wave at focus (e.g. crest, trough or otherwise) and the relative position and size of the individual waves within the same wave group envelope. Such phase information is seldom if ever included in empirical relationships used for predicting bulk overtopping volumes during irregular wave incidence, where its importance may be diluted owing to the random nature of the field. However for a single extreme event, phase may play a key role in response optimisation (Whittaker et al., 2017).

4. Wave overtopping and horizontal forces within the OXBOU model

Seawall overtopping in the laboratory wave flume is numerically modelled using a 1DH hybrid Boussinesq-nonlinear shallow water model. A comprehensive description of the model and extensive validation studies for a variety of runup and overtopping scenarios is presented by Orszaghova (2011) and Orszaghova et al. (2012). A brief overview is provided below. It should be noted that generation of the focused wave group was implemented numerically using a full second-order correction of the linear paddle signal whereas it was possible to achieve only partial second-order correction with the laboratory wavemaker.

The numerical wave flume, referred to as OXBOU, models pre-breaking and post-breaking free-surface flows, with occurrence of breaking and the associated breaking location determined by a criterion based on local free-surface slope. Weakly nonlinear, weakly dispersive Boussinesq equations with improved dispersion properties (Madsen et al., 1991; Madsen and Sørensen, 1992) are employed to model the smoothly varying non-breaking waves. Breaking is triggered when a critical free-surface slope is exceeded. Broken waves are modelled as bores using the nonlinear shallow water (NLSW) equations. Wave breaking is modelled by ramping the frequency dispersion terms in the Boussinesq-type equations down to zero over a quarter of a wavelength offshore of the designated breaking wave. The breaking location, which determines where the equations (gradually) switch from Boussinesq to NLSW, is recalculated at every time-step allowing the breaking waves to be tracked inshore; the Boussinesq equations can then be re-established at the original break point prior to the onset of further breaking.

The hybrid model incorporates a moving boundary piston wavemaker which replicates piston paddle wave generation in physical wave flumes. The implementation of a local bed modification approach in the wetting and drying treatment in the Godunov-type finite volume scheme, detailed elsewhere by Liang and Borthwick (2009), prevents spurious flow features at the wet-dry interface. Such a treatment allows for separation of the water mass into disjoint bodies of water which can evolve independently as might occur in an overtopping event. Thus, the finite volume solution scheme provides a robust method for simulating overtopping flows and can also be utilised for simulating dam-break or dike-failure scenarios. Simultaneous calculation of the solution inshore and offshore of the overtopped structure is obtained directly with the model. The overtopping volume (per unit width) is obtained by simple numerical integration: the water depth in each cell is multiplied by the corresponding cell length and summed over all cells inshore of the seawall crest.

4.1. Calculation of horizontal forces

In the hybrid model any moderate-to-large waves incident on the seawall will have broken before arrival at the front seawall slope so that NLSW equations will describe the overtopping interaction. Within a standard shallow water equation description, the vertical acceleration of the fluid is neglected, the pressure is purely hydrostatic, and so forces computed by integrating the pressure will have no hydrodynamic contribution. Therefore, an integral pressure force approach in the NLSW can only account for hydrostatic loads. Herein we determine the global horizontal load on the seawall using an approach based on the horizontal momentum flux ρq and fluid impulse arguments that inherently accounts for the hydrodynamic effect. Here the horizontal fluid impulse I of a wave group flow field in a 1DH domain of infinite extent is the integral of the momentum flux over the entire domain, i.e.

$$I = \int_{-\infty}^{\infty} \rho q \, dx. \tag{2}$$

In such a 1-D flow, the momentum, impulse, and force quantities are all per unit width. Therefore, the force exerted by the fluid on the wetted portion of the domain is given by

$$F = \frac{dI}{dt} = \frac{d}{dt}\int_{-\infty}^{\infty} \rho q \, dx. \tag{3}$$

Time derivatives of q are computed as part of the time integration procedure in the shallow water model and so the instantaneous horizontal force exerted by the fluid on the shallow water flume domain $\mathscr{D}$ is computed at each time step in the model from

$$F = \rho \int_{\mathscr{D}} \frac{dq}{dt} \, dx, \tag{4}$$

using numerical integration. Equation (4) provides the force on the entire wetted domain and not just on the seawall. In order to determine accurately the force on the seawall (within the constraints of the shallow water flow model), it is necessary to subtract the force on a domain in the absence of the seawall. More precisely, we seek the force on the front face of the seawall, while neglecting any sloshing occurring in the catchment region beyond the seawall. Therefore, it is necessary to compute the forces in two shallow wave flumes, one with an extended seawall and the other with an extended beach. Fig. 3 illustrates the extended geometries. In both cases, the horizontal end zones are implemented with zero friction and an open boundary condition is imposed at the right hand boundary of the domain to prevent flow reflection occurring. The horizontal force imparted to the seawall front by a prescribed wave group is then given by

$$F_{seawall} = -\rho\left(\int_{\mathscr{D}} \frac{dq}{dt} \, dx - \int_{\mathscr{D}_B} \frac{dq_B}{dt} \, dx\right), \tag{5}$$

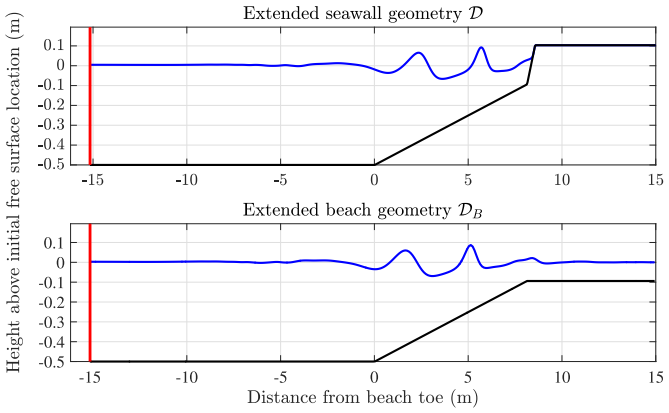

Fig. 3. Extended seawall and beach geometries used in calculation of seawall force.

where q is the velocity flux and $\mathscr{D}$ is the domain in the extended seawall interaction, and q_B is the velocity flux and $\mathscr{D}_B$ the domain in the extended beach interaction, with identical paddle driving signals in each case.

Forces calculated using the fluid impulse method are validated by comparison with the horizontal load cell measurements. For the purposes of verification, the wave load on the seawall resulting from perturbations in the purely hydrostatic pressure is also computed and compared to the forces obtained using the fluid impulse method described above. The hydrostatic load is calculated by integrating the perturbed hydrostatic pressure $\rho g\zeta$ from the seawall toe to the wave runup location on the seawall at every time step, i.e.

$$F_H = \left(\int_{\mathscr{D}_{WSW}} \rho g\zeta \; dx\right)\tan\alpha, \tag{6}$$

where $\mathscr{D}_{WSW}$ denotes the time-varying wetted seawall domain and $\zeta = h(x,t) - h_{SW}(x)$ where h and h_{SW} are the instantaneous water depth and still water depth, respectively. In order to obtain the horizontal component we simply multiply by the seawall slope, $\tan\alpha = 1/2.18$.

4.2. Validation of numerical model

The numerical model utilises two tunable parameters which can significantly influence the flow in the shallow water region of the domain: the threshold free-surface slope (which triggers breaking when exceeded) and the quadratic bed friction coefficient. Whittaker et al. (2017) previously calibrated these parameters based on runup measurements from the COAST flume (described in Section 2.1) for the same beach geometry in the absence of the seawall. They found that a threshold wave surface slope limit of 0.4 and a bed friction coefficient of $C_f = 0.010$ (where the bed friction source term in the momentum flux equation is $\tau_b = \rho C_f u|u|$ for a horizontal velocity u) gave the best agreement between numerical predictions and laboratory measurements. These values are utilised in the seawall overtopping simulations that follow.

Model validation is achieved by comparing the predicted and measured free-surface elevation time series at different locations along the flume and overtopping volumes for a single focused wave group overtopping test. This particular focused wave group, of linear focus amplitude $A = 0.0855$ m, focus location relative to the beach toe $x_f = 5.0$ m, and phase at focus $\phi = 180°$, was chosen because it produces a large overtopping event. Fig. 4 shows the excellent agreement between the predicted and measured free-surface elevations at the ten wave gauges located between the wavemaker and the seawall toe. Slight under-prediction of the wave crest amplitudes is however evident, particularly from gauge 6 to gauge 8 where the waves shoal on the beach, and the predicted troughs of the waves at the centre of the group

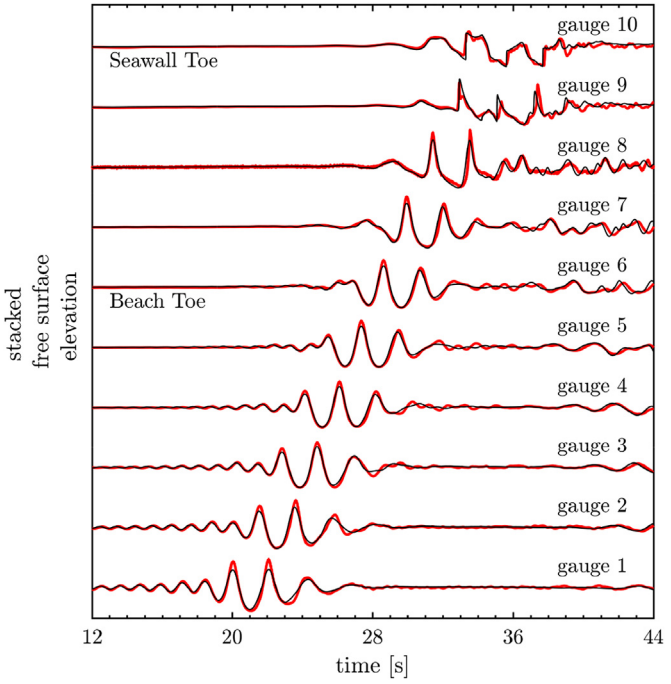

Fig. 4. Free-surface elevations at ten wave gauges as far as the seawall toe (see Fig. 1 for gauge locations) of a focused wave group producing large overtopping volumes; measured (red) and OXBOU predicted (black). (For interpretation of the references to colour in this figure legend, the reader is referred to the web version of this article.)

appear lower than measured at gauges 7 and 8. The discrepancies are attributed to the weakly nonlinear nature of the Madsen and Sørensen Boussinesq equations and to the partial correction of the second-order error wave by the laboratory wavemaker.

A pair of wave gauges measured bores that ran up the face of the seawall and overtopped the seawall crest. The first gauge was located at the seaward edge of the crest and the second at the mid-point of the crest; these gauges are shown in Fig. 1. Fig. 5 compares OXBOU predictions of the overtopping bore elevations on the seawall against those from these two gauges. The numerical predictions and laboratory measurements exhibit close agreement for the first, largest peak at time $t \sim 34$ s (confirming experimental repeatability and validating the

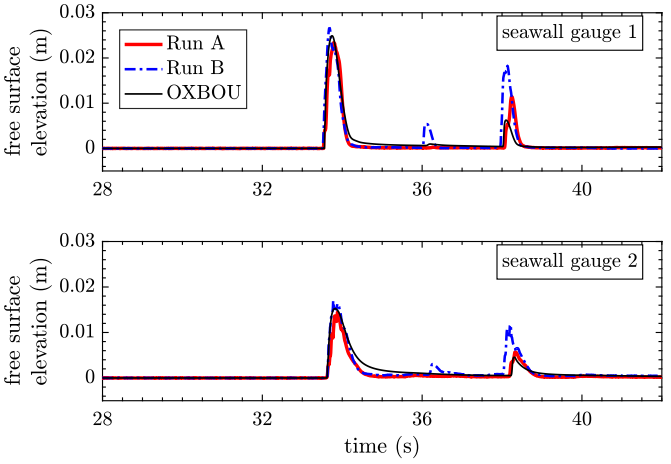

Fig. 5. Free-surface elevation time-histories by seawall gauges 1 and 2 (corresponding to wave gauges 11 and 12 in Fig. 1), located at the most seaward and central points on the seawall crest; laboratory measurements (red, blue) and OXBOU predictions (black). $A = 0.0855$ m, $x_f = 5.0$ m relative to the beach toe, $\phi = 180°$.

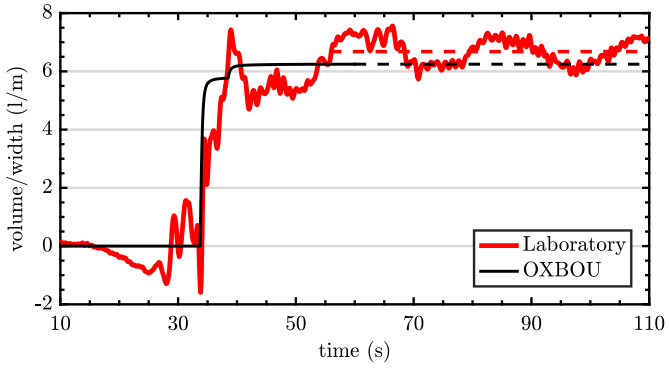

Fig. 6. Overtopping volumes per unit width measured by the overtopping receptacle load cell (red) and predicted by OXBOU (black). The total volume measured by the overtopping receptacle load cell is shown by the dashed red line. $A = 0.0855$ m, $x_f = 5.0$ m relative to the beach toe, $\phi = 180°$. (For interpretation of the references to colour in this figure legend, the reader is referred to the web version of this article.)

numerical model) but significant discrepancies are evident between the repeat experimental data for the second largest peak at time $t \sim 38$ s. Such discrepancies between the repeat test measurements can be attributed to the physics of the broken waves travelling on aerated and fully turbulent bores.

Fig. 6 displays predicted and measured overtopping volume time-histories. Sloshing by overtopped water within the receptacle and its natural motion resulted in oscillations in the volume measurements about the total overtopped volume after water entry in the receptacle. Agreement between the numerical and physical overtopping volume time histories is satisfactory, with a 7% difference in final volume. A probable cause of this discrepancy is the imperfect removal of low frequency error waves in the laboratory tests.

Fig. 7 shows the horizontal force time histories obtained for the same focused wave group ($A = 0.0855$ m, $x_f = 5.0$ m relative to beach toe, $\phi = 180°$) as considered previously. All forces (and pressures, volumes etc.) obtained from the 1-D shallow water model are per unit width and so the horizontal load cell measurements were divided by the width of the force panel. Fig. 7 illustrates the extent of the agreement between the numerical predictions and laboratory measurements of the horizontal force per unit width. The alignment in time of the predicted and measured maxima is excellent for both hydrostatic pressure and fluid impulse derived forces. Satisfactory agreement is achieved regarding the magnitude of the horizontal force oscillations. However, the OXBOU predictions yield a noticeably larger global maximum than

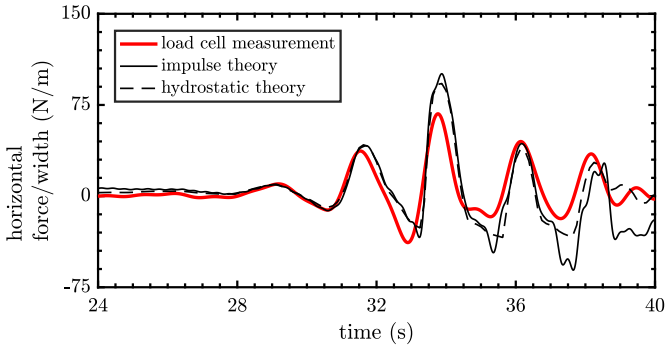

Fig. 7. Horizontal force per unit width measured by the horizontal load cell (red) and predicted numerically by OXBOU using the total force impulse and hydrostatic (solid black) and hydrostatic pressure alone (dashed black) methods for partial second-order corrected wave generation in OXBOU. $A = 0.0855$ m, $x_f = 5.0$ m relative to the beach toe, $\phi = 180°$. (For interpretation of the references to colour in this figure legend, the reader is referred to the web version of this article.)

measured. This may be attributed to bearing effects at the end of the seawall, the sealant around the force panel, the wet-backed nature of the seawall or to the limitations of the numerical model in simulating a complicated physical event. The load cell measurements can be affected also by the (possible) high stiffness of the load cell itself, compared to the order of magnitude of the expected forces. Fig. 7 also shows how the hydrostatic pressure integral over the wetted seawall can provide an excellent approximation to the fluid impulse method – which includes hydrodynamic terms within the limitations of the shallow water model – for (partially corrected) second-order focused wave groups. Similar agreement between the impulse-based and hydrostatic pressure force predictions was observed for several other focused wave group realisations. Therefore, we can conclude that the purely hydrostatic pressure integration method provides a good approximation to the total wave load for pulsating wave loads with low wave impact velocities and, based on the shallow water model fluid impulse computation, hydrodynamic contributions to the horizontal force are relatively small.

5. Overtopping volumes

5.1. Total overtopping volumes

We first conduct a thorough analysis of the laboratory measurements and numerical predictions of the total overtopping volumes for each incident focused wave group. Wave-by-wave overtopping volumes within each focused wave group are subsequently considered solely using numerical model predictions. For most practical purposes (e.g. when measuring overtopping during long periods of irregular wave incidence), the total overtopping volume for a compact group of waves is a sufficiently localised measurement (in time). Fig. 8 illustrates the parametric dependence of total overtopping volume on focus location and phase for NewWave focused wave groups of three different linear focus amplitudes. Both numerical and experimental total overtopping volumes are plotted using the same colour scale. Although this slightly obscures the response trends for the (smaller) numerical predictions, this consistent treatment highlights differences in predicted and measured overtopping volumes over the entire parameter space. The bands of large and small total overtopping discharges are emphasised by extending the range of phase angles at focus from (0°, 360°) to (−360°, 360°). The wave form is periodic with period 2π with respect to ϕ and so extending the contour plot is simply a matter of duplicating the overtopping results for $\phi \in (0°, 360°)$ to $\phi \in (-360°, 0°)$. Focus locations are defined relative to the beach toe in this and all subsequent parametric plots. Here, the seawall toe is located at a focus location 8.125 m and the still water shoreline in the absence of the wall corresponds to 10 m. Locations of the seawall toe and the start of the seawall crest are indicated with white lines in Fig. 8. For each linear focus wave amplitude considered in the parametric optimisation, the bands or ‘stripes’ of optimal total overtopping volumes are broadly similar in character. Maximum total overtopping volumes are induced by compact wave groups focusing in a region 5 m either side of the centre of the seawall, i.e. $x_f \in (3.7\text{ m}, 13.7\text{ m})$, for the two largest focus wave amplitudes. For the smallest focus wave amplitude ($A = 0.057$ m), the band of optimal overtopping responses is more diffuse than those associated with the larger amplitudes and appears largest in the region offshore of the seawall toe ($x_f \geq 8.125$ m). The total overtopping volume strongly depends on the phase angle of the wave group at focus. For the intermediate amplitude, $A = 0.0855$ m, it is predicted that a crest-focused wave group ($\phi = 0°$) focusing 10 m from the beach toe would produce approximately 9 l/m of overtopping volume in total. However, a trough-focused wave group ($\phi = 180°$) focused at the same point produces only 2 l/m of overtopping volume in total, less than a quarter of the previous (maximum) overtopping volume. Many empirical formulae for predicting overtopping discharges and volumes only incorporate spectral parameters such as significant wave height or peak period. At first sight this appears intuitively reasonable because

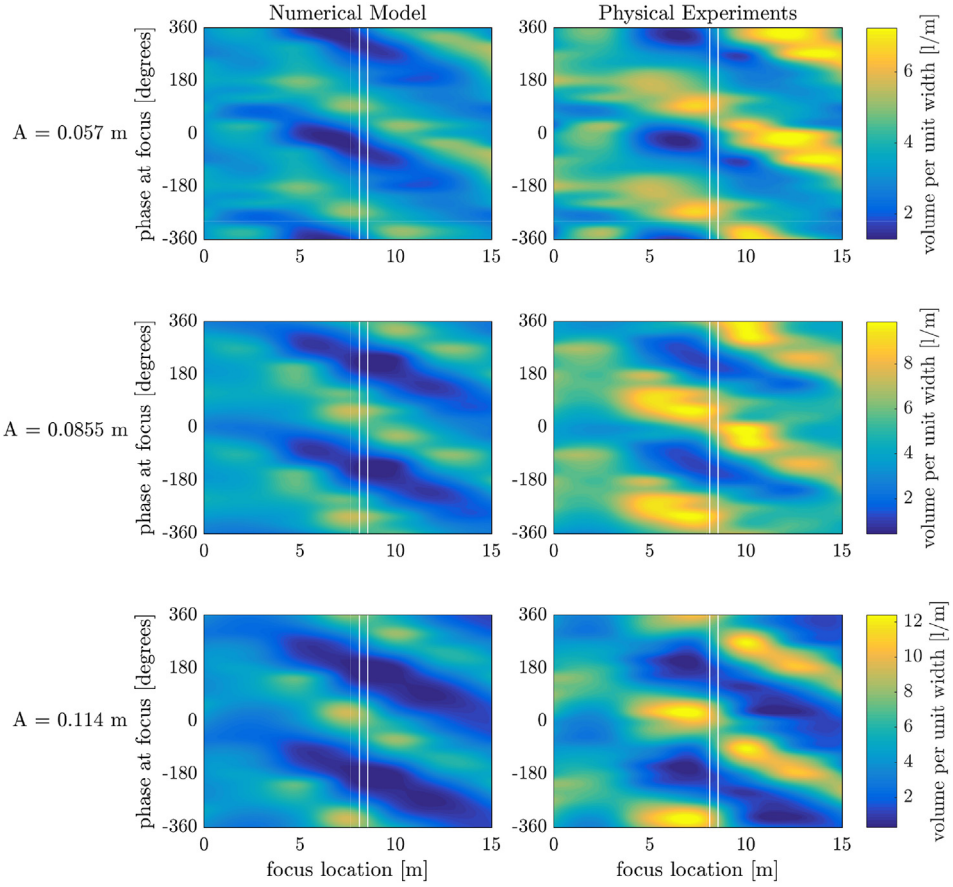

Fig. 8. Total overtopping volumes generated by incident focused wave groups with varying amplitude, focus location, and phase at focus. The white lines indicate the location of the seawall toe (leftmost) and the start of the seawall crest (rightmost).

crest- and trough-focused wave groups (or a wave group with any arbitrary phase) have the same wave envelope, and so the same concentration of energy arrives at the seawall regardless of phase. However, the parametric dependence of total overtopping volume given by Fig. 8 indicates that the phase of the waves is of crucial importance at least for focused wave groups. Although such phase dependence is likely to hold for large individual overtopping events under irregular wave attack, this was not considered in the current study.

Fig. 8 also confirms that maximum total overtopping volume increases monotonically with linear focused wave group amplitude. On the other hand, the *minimum* total overtopping volume for each parameter exhibits more nuanced, counter-intuitive behaviour (due to some waves within the group not overtopping at all). In fact, the minimum total overtopping volume decreases as the incident focused wave amplitude increases! The minimum total overtopping volumes over the (x_f, ϕ) parameter space for the focused wave groups of linear amplitudes $A = (0.057\text{ m}, 0.0855\text{ m}, 0.114\text{ m})$ were 1.85 l/m, 1.83 l/m, and 0.47 l/m, respectively. Similarly, the numerically predicted minimum overtopping volumes were calculated to be 1.28 l/m, 0.44 l/m and 0.31 l/m for the three increasing linear focus amplitudes. This somewhat complicated behaviour appears to be caused by the increased reflections from the steeper (compared to the beach) seawall slope. Large total overtopping volumes contain a significant contribution from the first wave in the group, according to numerical predictions, because this is unaffected by reflections. All subsequent waves suffer interference from reflected waves. Therefore, if the first wave achieves overtopping then subsequent waves are also more likely to overtop. However, if the first wave does not quite overtop the seawall then after strong reflection it may cause subsequent incoming waves to break prematurely, leading to significant net energy loss and reduction in total overtopping volume. The focused wave group conditions leading to large and small total overtopping volumes are examined in greater detail in Section 5.2.

Numerical predictions were made of the total overtopping volumes produced by focused wave groups generated using linear, partially-corrected and fully-corrected second-order wavemaker theory. The results (not shown here for brevity) are consistent with findings by Orszaghova et al. (2014) that focused wave groups generated using linear theory produce larger overtopping volumes than those generated using second-order theory. Furthermore, the over-estimation obtained from linear generation increases for larger linear wave amplitudes because the spurious second-order difference frequency wave generated at the paddle increases quadratically with linear wave amplitude. For a linear focus wave group of amplitude $A = 0.114$ m, the parametrically optimised values of total overtopping volume per unit width obtained using linear, partial second-order corrected and full second-order corrected wave generation theory (for an idealised piston paddle) are 13.4 l/m, 9.4 l/m and 8.5 l/m, respectively. An erroneous increase of 57% in overtopping volume occurs owing to spurious long wave generation. The linear wavemaker theory predictions for overtopping volumes are more comparable to the experimental measurements based on a partially-corrected second order EDL paddle motion. This suggests that either the numerical predictions systematically underestimate the overtopping volumes or that partial second-order generation implemented in the laboratory is less effective than noted by Whittaker et al. (2017). That is, partial second-order generation may reduce the amplitude of the long error wave by 60% locally (around the maximum) only; the most damaging (in terms of accuracy) portion of the long wave (the longest components) remains in the wrong place at the wrong time, leading to exaggerated estimates of the overtopping

Table 2
OXBOU predictions of focus locations and phases at focus leading to the maximum/minimum overtopping volumes for focused wave groups with $A = 0.0855$ m, where focus locations are given relative to the beach toe.

Focus location (m)	V_{max} (l/m)	Phase for V_{max} (°)	V_{min} (l/m)	Phase for V_{min} (°)
7.5	6.8	60	0.68	255
10.0	6.5	270	0.28	225
12.5	5.5	255	0.73	120

volume.

5.2. Parametrically optimised focused wave groups for maximum and minimum seawall overtopping

Numerical simulations were conducted with full second-order generation to examine focused wave group conditions that yield maximum and minimum overtopping volumes for a single linear focus amplitude ($A = 0.0855$ m). Table 2 lists the phase values which yield the maximum and minimum overtopping responses at three different focus locations. These (x_f, ϕ) combinations correspond to points in the bands of large (or small) overtopping volumes displayed in Fig. 8, now using the full second-order corrected wavemaker signals. Note that the minimum overtopping volume predicted by the numerical model for second-order generated focused wave groups is significantly smaller than that obtained from the laboratory measurements in Section 5.1 owing to the partial implementation of the second-order correction to the laboratory wavemaker. Here, the effect of the (partially suppressed) error wave is to enhance artificially all overtoppings by the focused wave groups.

Fig. 9 presents the free-surface elevation time-histories at the beach toe, 5.0 m inshore of the beach toe (referred to as mid-beach), and 0.625 m offshore of the seawall toe (7.5 m inshore of the beach toe, referred to as upper beach) for focused wave groups with x_f and ϕ values listed in Table 2. Overtopping volume time histories are also displayed so that the overtopping responses at the seawall can be directly related to the evolution of each wave group during shoaling. Free-surface elevation and overtopping time-histories are time-shifted so that the instant of maximum overtopping discharge (i.e. the instant at which the overtopping rate is greatest) coincides for all wave groups at the time origin. The optimised focused wave groups in Fig. 9 exhibit striking similarity; those wave groups correspond to the band of high overtopping volumes in the contour plot in Fig. 8 at focus locations $x_f = (7.5\text{ m}, 10.0\text{ m}, 12.5\text{ m})$. As the focused waves propagate inshore, the wave preceding the main group of three waves remains small (corresponding to the small hump that can be discerned at $t = -5.0$ s at mid-beach, and $t = -3.0$ s at the seawall toe) and causes no overtopping discharge. In all cases, all overtopping occurs upon incidence of the first wave crest in the main wave packet, i.e. the crest that passes mid-beach at approximately $t = -2.5$ s and the upper beach at $t = -1.0$ s. A slight secondary overtopping event occurs for the $x_f = 12.5$ m focused wave at $t = -2.5$ s, but is difficult to distinguish in Fig. 9. The main overtopping event for this wave group is correspondingly smaller than its counterpart at focus locations 7.5 m and 10.0 m from the beach toe.

A cursory comparison between the results for wave groups (de)tuned for minimum overtopping to those for maximum overtopping reveals how the increase in amplitude of the leading wave diminishes the primary overtopping event. This primary overtopping event occurs when the largest wave crest reaches the front of the seawall. However, its magnitude is significantly reduced through interference by the reflected leading wave interaction with the seawall. From Fig. 9, it appears that the overtopping wave crests (circled) at mid-beach are approximately equal in amplitude for both types of optimised wave group. However, at the seawall toe the overtopping bore height is greater for

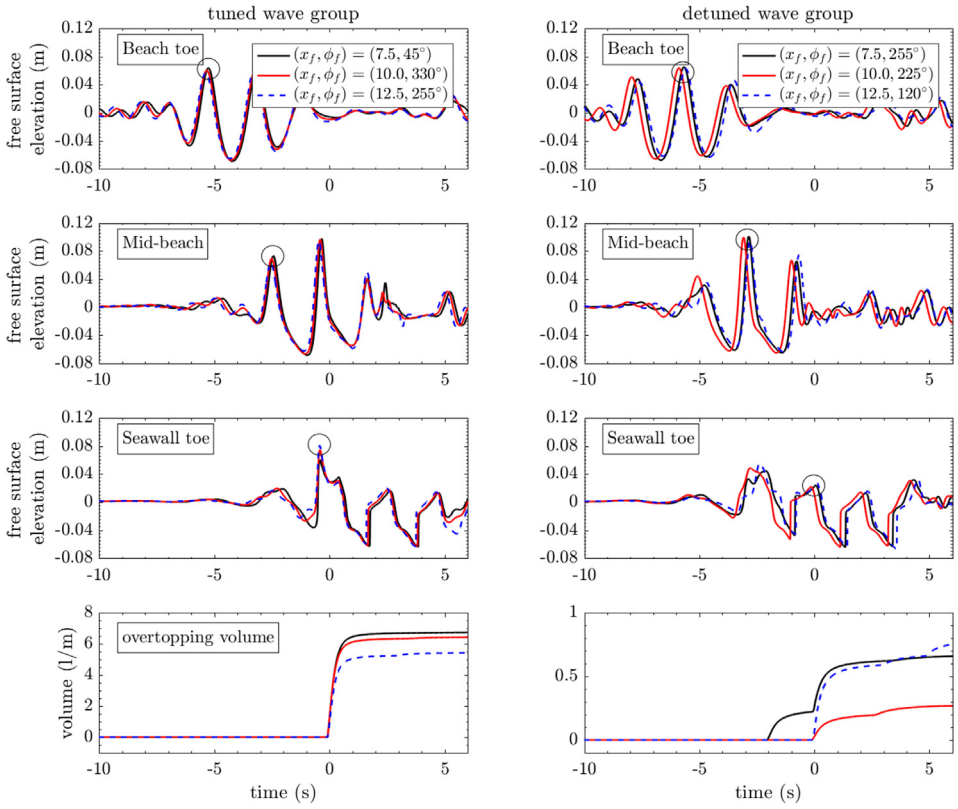

Fig. 9. Free-surface elevation time series at three beach locations and overtopping volume time histories for a focused wave group with linear focus amplitude of $A = 0.0855$ m with incident wave conditions leading to maximum (left column) and minimum (right column) total overtopping volumes. The circled wave crest at each location causes the primary overtopping event. Note the scales of the overtopping volume plot differ by a factor of 8 to improve clarity of the 'detuned' case.

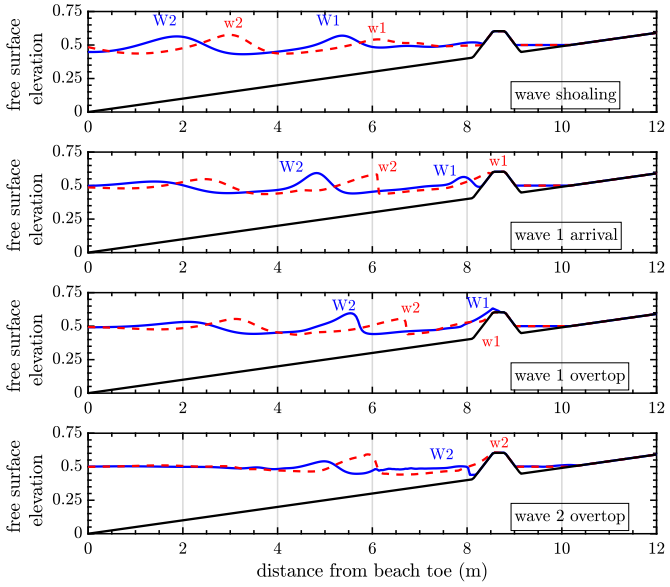

Fig. 10. Free-surface elevation profiles at the seawall at four different times for the focused wave groups with focus location $x_f = 10.0$ m and phases $\phi = -30°$ (blue, upper-case 'W') and $\phi = 225°$ (red dashed line, lower-case 'w'), which induce very large and small overtopping volumes, respectively, for a linear focus amplitude of 0.0855 m. (For interpretation of the references to colour in this figure legend, the reader is referred to the web version of this article.)

the wave group optimised for large overtopping. In the upper beach region, bore height reduction of the overtopping wave in the detuned wave group occurs because of premature breaking caused by either direct interaction with the reflected leading wave or losses associated with additional breaking due to the foregoing reflected wave. Multiple overtopping events, which contribute similar overtopping volumes to the rather small totals, occur in the 'detuned' overtopping time-histories shown in Fig. 9.

Fig. 10 compares the free-surface elevation profiles of phase-optimised wave groups for large and small overtopping events at four instants as the focused wave arrives at the seawall. Both wave groups are listed in Table 2 and correspond to a linear focus amplitude $A = 0.0855$ m and focus location $x_f = 10.0$ m inshore of the beach toe. At time $t = 28.0$ s, the wave group inducing very little overtopping (green) possesses a small crest denoted w1 a distance of 6 m inshore of the beach toe, followed by a much larger crest (w2) 3 m inshore of the beach toe. w1 runs up the seawall at $t = 29.75$ s and almost overtops the crest of the seawall before w1 runs down the seawall and reflects offshore at $t = 30.125$ s. A small trough forms at the seawall after rundown, and coupled with the interference caused by the reflected wave, very little overtopping occurs at $t \simeq 32$ s upon arrival of w2. Additional overtopping occurs as the wave crest located 6 m inshore of the beach toe in the last snapshot (also incorporating some reflected wave contributions) is incident on the seawall. In contrast, the wave group locally optimised for large overtopping suffers negligible reflection interference because of the small leading crest incident on the seawall at $t = 28.0$ s. Significant overtopping occurs as W1 is incident on the seawall at $t = 30.125$ s. W2 undergoes breaking just after this time and the resultant energy losses mean no additional overtopping occurs upon arrival at the seawall. For the compact focused wave group envelope considered herein the overtopping response is maximised when reflections from the leading waves are minimised. Furthermore, maximum overtopping volumes correspond to a single large overtopping event, whereas overtopping volumes due to multiple consecutive overtopping events are significantly smaller. This behaviour is evident in all overtopping experiments and simulations recorded in this study. Overtopping volumes for the wave groups tuned for minimal

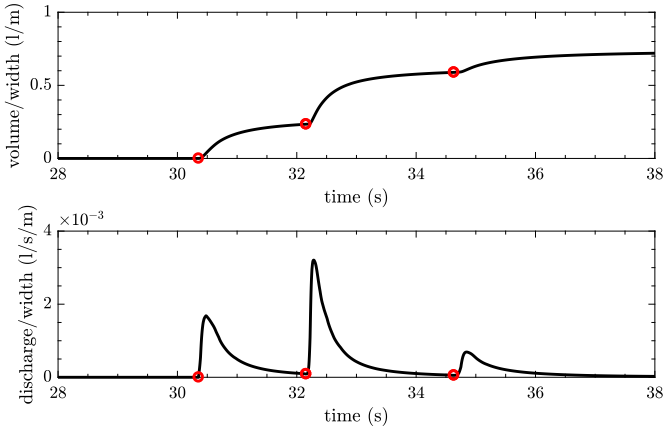

Fig. 11. Overtopping volume and discharge time histories for a focused wave group of amplitude 0.0855 m, focus location 10.0 m from the beach toe, and phase angle at focus of 120°.

overtopping are an order of magnitude smaller than for the wave groups tuned for maximal overtopping — an indication of just how sensitive focused wave group total overtopping volumes are to the wave group phase angle.

5.3. Maximum individual overtopping volumes

Thus far, we have analysed the measured and predicted total overtopping volume for an incident wave group. This overtopping response is measured over similar time scales to the individual wave-by-wave overtopping response for compact focused wave groups. Therefore, it is expected that the total group overtopping volume will agree closely with the maximum individual wave overtopped volume.

In order to identify the maximum individual overtopped response from the overtopping volume time history, each overtopping contribution must be identified and separated. This can be done in a straightforward manner for the numerical predictions where no sloshing occurs and the volume time history increases steadily with each additional wave overtopping event. In such cases, the volume contributions may be divided according to the instants when the overtopping discharge increases (as denoted by the red circles in Fig. 11). In this example, three distinct overtopping events occur and the total overtopped volume (0.74 l/m) is approximately twice the maximum individual volume (0.35 l/m). Such behaviour is common for focus locations and phases that yield very small total overtopping volumes, as illustrated in Fig. 9. However, a single significant overtopping event contributes most of the total overtopping volume for the focused wave groups considered herein, inducing medium-to-large overtopping volumes as shown in Fig. 9. Therefore, it is unsurprising that only small differences are evident when the maximum individual overtopping volume response and total wave group overtopping volume response are compared, as shown in Fig. 12.

6. Horizontal forces exerted on seawall

6.1. Parametric optimisation of horizontal forces

Fig. 13 shows the numerically predicted (from fluid impulse derivatives) and experimentally measured maximum horizontal forces (per unit width) exerted by focused wave groups on the seawall for varying focus location and phase. Different colour scales are utilised for the numerical and experimental force contour plots for the same linear focus wave envelope amplitudes owing to the discrepancy in maximum horizontal force amplitude (as evident in Fig. 7). The largest maximum horizontal force measured over the focused wave parameter space is observed to be approximately two-thirds the corresponding numerical

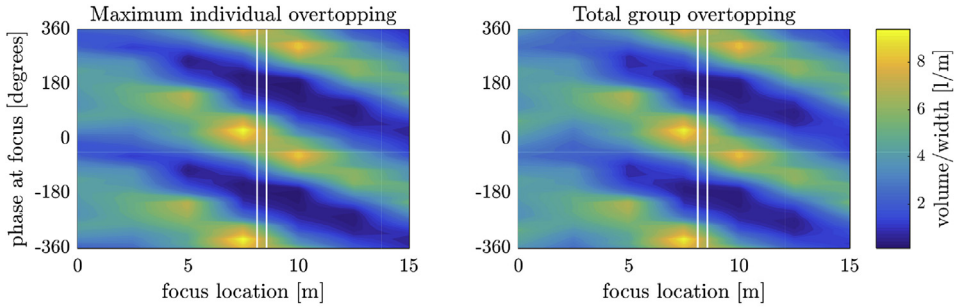

Fig. 12. Maximum overtopping volumes generated by incident focused wave groups of amplitude 0.114 m for varying focus location and phase at focus.

prediction for all linear focus wave amplitudes. Nevertheless, similar bands of large and small maximum force response (represented by light and dark areas respectively) are evident in Fig. 13 at all amplitudes for both the horizontal load cell measurements and the fluid impulse derivative predictions. This implies that the sensitivity of the force response to changes in focus location and phase at focus is quite similar for all focus wave amplitudes. However, interpolation of the experimental data across focus locations $x_f = 2.5$ m and $x_f = 7.5$ m based on the numerical contours appears to have artificially shaped the force contour plots in some cases. For example, the existence of (weak) areas of large response at $x_f = 2.5$ m and $x_f = 7.5$ m in the contour plots for the two largest amplitudes does not appear consistent with the behaviour at $x_f = 0$ m and $x_f = 5.0$ m where the behaviour is determined by actual laboratory measurements.

Agreement between measurements and predictions appears to be best for the intermediate amplitude focused waves ($A = 0.0855$ m). And the NLSW model might be expected to provide a good approximation to the momentum and impulse changes occurring in the flow around the seawall for gentle wave interactions where the impulsive component of the flow is small. However, reasonably similar behaviour of the maximum horizontal force over the focus wave location/phase parameter space is also evident for the largest focus wave amplitude. This suggests that the seawall experiences predominantly pulsating wave loads even when under attack by relatively large waves, owing to the beach and seawall geometries; the seawall slope is relatively gentle and, as noted previously, is similar to that of a dike.

Total overtopping and maximum horizontal force seawall responses have been constructed across the entire focused wave parameter space from numerical predictions and laboratory measurements as illustrated in Figs. 8 and 13. Inspection of the bands of large and small responses obtained from the laboratory measurements of the overtopping and horizontal force responses reveal certain similarities: the positions of light and dark bands within the parameter space are very similar for both responses. This broadly indicates that a large overtopping event coincides with a large horizontal load on the sloped seawall. As previously noted, however, the total overtopping volumes vary to a far greater extent than the maximum horizontal loads. The similarity in response implies that the maximum horizontal force on the seawall increases as the volume of water surging up and over the seawall slope increases, at least for this particular focused wave group. This is not surprising if we consider the forces on the seawall as being largely hydrostatic (as appears to be the case from Fig. 7). Large hydrostatic

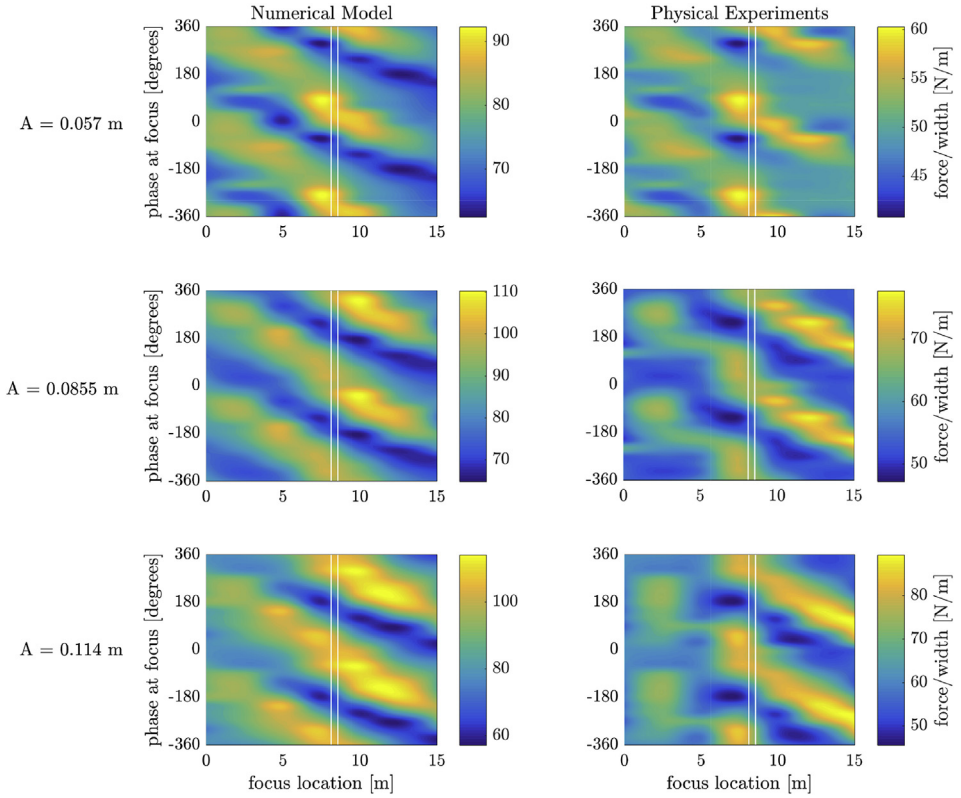

Fig. 13. Maximum horizontal forces exerted on the seawall by incident focused wave groups with varying amplitude, focus location, and phase at focus.

pressures and large overtopping volumes both require similar wave conditions; i.e. a large net displacement of water above the mean water line from the seawall toe to the crest of the seawall. Given that the first wave to overtop the seawall also provided the largest contribution to the horizontal force (see Figs. 5 and 7), it seems that minimal reflection of the preceding wave is a prerequisite in maximising both the overtopped volume and the horizontal force on the seawall. Discrepancies are also evident, for the two largest focused wave envelope amplitudes at least, where the largest maximum horizontal forces (for a given phase) occur for wave groups focused farther inshore than for the total overtopping volumes. This may indicate a slight positive phase shift is required to change from the maximum overtopping volume to the maximum horizontal force at a given focus location (possibly due to the phasing of the free surface elevation relative to the horizontal velocity).

Lastly, we compare the properties of the focused wave groups tuned for largest and smallest maximum horizontal loads and total overtopping volumes based on numerical predictions for a linear focus amplitude of 0.0855 m. Table 2 provides details of the tuned and detuned overtopping focused wave group specifications considered for this amplitude. More specifically, we determine the focused wave phase angle that induces the locally maximum horizontal load at the three focus locations nearest the seawall crest (i.e. $x_f = 7.5$ m, $x_f = 10.0$ m, and $x_f = 12.5$ m). However, it should be noted that the globally maximum horizontal seawall force occurs farther inshore in the parametric optimisation based on the horizontal load cell measurements — the band of large horizontal force responses is observed for focus locations inshore of the seawall, that is for $x_f \in (9.0\text{ m}, 15.0\text{ m})$, for the two largest focused wave group amplitudes. Such onshore focus locations may suppress breaking before the wave group arrives at the seawall, so that the waves may break (spilling) on the seawall thus inducing the largest force on the seawall. Nevertheless, the focused wave groups inducing the largest maximum horizontal load at $x_f = 7.5$ m, 10 m, 12.5 m are found to have phases of $\phi = 45°, 315°, 225°$. These largely coincide with phases yielding the largest overtopping volumes listed in Table 2 ($\phi = 60°, 270°, 255°$). Wave groups yielding the smallest maximum horizontal force for the three focus locations $x_f = 7.5$ m, 10.0 m, 12.5 m possess similar but not identical phases ($\phi = 255°, 180°, 120°$) compared to the 'detuned' focused wave groups with small overtopping responses listed in Table 2 ($\phi = 255°, 225°, 120°$).

Whittaker et al. (2017) also tuned the group phase to induce optimal runup on the underlying plane beach geometry used in the seawall experiments (where the beach extends beyond still water level) for the same focused wave group amplitude and focus locations listed in Table 2. Their findings indicate that the same tuned wave groups will give optimal runup and overtopping for this particular seawall geometry and configuration. In summary, wave groups tuned to give large runup, overtopping, and force responses for focus locations around the still water level or seawall are almost identical for this wave group and the beach and seawall geometries.

7. Conclusions

For each overtopping interaction involving a gently-sloped (1/2.18) seawall on a 1/20 foreshore beach slope, high temporal-resolution measurements were obtained of free-surface elevation, overtopping volume, and seawall load. The scope of the laboratory parametric investigations was broadened (to include finer parameter space discretisations and alternative wavemaker theories) by application of a validated Boussinesq-shallow water model. Erroneous increases in overtopping of up to 57% caused by utilising linear paddle signals instead of second-order corrected paddle signals were predicted numerically for the largest focused wave group, consistent with the findings of Orszaghova et al. (2014). This result implies that empirical relationships based on experiments conducted using linear wave generation may be overly conservative, since the presence of error waves would have artificially increased the overtopping during these experiments. Overtopping events parametrically optimised for large and small overtopping events were investigated at a higher spatial resolution in the numerical simulations thus providing valuable insights into conditions leading to extreme responses.

Total group overtopping volumes exhibited a strong dependence on focus location, linear amplitude and phase of the group at focus. For a given linear amplitude and focus location, changing the phase of the group at focus could lead to an order of magnitude increase in the total overtopped volume. This strong phase dependence may help explain the variation in some of the overtopping results previously reported in the literature. The maximum overtopping volume occurred when the size of the first overtopping bore was maximised compared to the preceding and following non-overtopping bores. Different combinations of phase and focus location generated this large leading bore at each of the linear group amplitudes tested, resulting in 'bands' of optimised overtopping volume for each amplitude. Conversely, the minimum overtopping volume was obtained by maximising the size of the preceding non-overtopping bore, because the downrush of this bore significantly reduced the momentum of the (subsequent) overtopping bores. Free-surface profiles obtained from the numerical simulations allowed detailed analysis of overtopping on a wave-by-wave basis. Furthermore, numerical predictions of the overtopping volume time-history were easily separated into wave-by-wave contributions (unlike the laboratory measurements, which were affected by the dynamic entry of water into the overtopping receptacle). Parametric dependence of the maximum individual wave overtopping volumes strongly resembled that of the total group overtopping volume, confirming the importance of the first overtopping wave in determining the total group overtopping. On the other hand, wave groups inducing very small total overtopping volumes typically involved two or three overtopping events of similar magnitude. Numerical predictions of horizontal seawall force were obtained using two methods: fluid impulse arguments (incorporating some hydrodynamics) and integration of the perturbed hydrostatic pressure. Within the framework of the nonlinear shallow water model, the hydrodynamic contributions are sufficiently small that the perturbed hydrostatic pressure force gives an accurate approximation to the pulsating horizontal force on the gently sloped seawall. For seawalls with steeper slopes, it seems likely that hydrodynamic contributions to the horizontal load will increase in importance, particularly in the extreme case of breaking wave impacts. The predicted forces exhibited good agreement with the measured forces.

The maximum horizontal force and total overtopping volume exhibited similar dependence on the phase, focus location and amplitude of the incident focus wave group. This parametric dependence contained clear 'bands' of large and small values as a function of phase and focus location (for a given amplitude). Although these bands are slightly phase-shifted between the two types of responses, the striking similarity between these two response types (and with the parametric dependence of runup on a plane beach reported by Whittaker et al., 2017) demonstrates the versatility of the focused wave parametric optimisation approach used in this study for a range of important coastal responses.

Acknowledgements

This work was conducted within the ENFORCE (Extreme Responses using NewWave: Forces, Overtopping and Runup in Coastal Engineering) project, under EPSRC Grant EP/K024108/1.

Appendix A. Supplementary data

Supplementary data related to this article can be found at https://doi.org/10.1016/j.coastaleng.2018.08.004.

References

Akbari, H., 2017. Simulation of wave overtopping using an improved SPH method. Coast. Eng. 126, 51–68.

Allsop, N., Vicinanza, D., Calabrese, M., Centurioni, L., et al., 1996. Breaking wave impact loads on vertical faces. In: The Sixth International Offshore and Polar Engineering Conference. International Society of Offshore and Polar Engineers.

Allsop, N., Bruce, T., Pearson, J., Alderson, J., Pullen, T., 2003. Violent wave overtopping at the coast, when are we safe? In: Proceedings of the International Conference on Coastal Management 2003. Institution of Civil Engineers, pp. 54–69.

Altomare, C., Suzuki, T., Chen, X., Verwaest, T., Kortenhaus, A., 2016. Wave overtopping of sea dikes with very shallow foreshores. Coast. Eng. 116, 236–257.

Boccotti, P., 1983. Some new results on statistical properties of wind waves. Appl. Ocean Res. 5, 134–140.

Borthwick, A.G.L., Hunt, A.C., Feng, T., Taylor, P.H., Stansby, P.K., 2006. Flow kinematics of focused wave groups on a plane beach in the U.K. Coastal Research Facility. Coast. Eng. 53, 1033–1044.

Briganti, R., Bellotti, G., Franco, L., Rouck, J.D., Geeraerts, J., 2005. Field measurements of wave overtopping at the rubble mound breakwater of Rome-Ostia yacht harbour. Coast. Eng. 52, 1155–1174.

Bruce, T., van der Meer, J., Franco, L., Pearson, J., 2009. Overtopping performance of different armour units for rubble mound breakwaters. Coast. Eng. 56, 166–179 The CLASH Project.

Castellino, M., Sammarco, P., Romano, A., Martinelli, L., Ruol, P., Franco, L., Girolamo, P.D., 2018. Large impulsive forces on recurved parapets under non-breaking waves. a numerical study. Coast. Eng. 136, 1–15.

Chen, X., Hofland, B., Altomare, C., Suzuki, T., Uijttewaal, W., 2015. Forces on a vertical wall on a dike crest due to overtopping flow. Coast. Eng. 95, 94–104.

Chen, X., Hofland, B., Uijttewaal, W., 2016. Maximum overtopping forces on a dike-mounted wall with a shallow foreshore. Coast. Eng. 116, 89–102.

Cuomo, G., Allsop, W., Bruce, T., Pearson, J., 2010. Breaking wave loads at vertical seawalls and breakwaters. Coast. Eng. 57, 424–439.

Dalrymple, R., Rogers, B., 2006. Numerical modeling of water waves with the SPH method. Coast. Eng. 53, 141–147 Coastal Hydrodynamics and Morphodynamics.

Franco, L., Geeraerts, J., Briganti, R., Willems, M., Bellotti, G., Rouck, J.D., 2009. Prototype measurements and small-scale model tests of wave overtopping at shallow rubble-mound breakwaters: the Ostia-Rome yacht harbour case. Coast. Eng. 56, 154–165 The CLASH Project.

Geeraerts, J., Troch, P., Rouck, J.D., Verhaeghe, H., Bouma, J., 2007. Wave overtopping at coastal structures: prediction tools and related hazard analysis. J. Clean. Prod. 15, 1514–1521.

Goda, Y., 2009. Derivation of unified wave overtopping formulas for seawalls with smooth, impermeable surfaces based on selected CLASH datasets. Coast. Eng. 56, 385–399.

Gomez-Gesteira, M., Cerqueiro, D., Crespo, C., Dalrymple, R., 2005. Green water overtopping analyzed with a SPH model. Ocean Eng. 32, 223–238.

Higuera, P., Lara, J.L., Losada, I.J., 2013. Simulating coastal engineering processes with OpenFOAM®. Coast. Eng. 71, 119–134.

Higuera, P., Lara, J.L., Losada, I.J., 2014a. Three-dimensional interaction of waves and porous coastal structures using OpenFOAM®. Part I: formulation and validation. Coast. Eng. 83, 243–258.

Higuera, P., Lara, J.L., Losada, I.J., 2014b. Three-dimensional interaction of waves and porous coastal structures using openfoam®. Part II: Application. Coast. Eng. 83, 259–270.

Hofland, B., Wenneker, I., Van Steeg, P., 2014. Short test durations for wave overtopping experiments. In: Proceedings of the 5th International Conference on the Application of Physical Modelling to Port and Coastal Protection, Varna, Bulgaria, pp. 349–358.

Hofland, B., Diamantidou, E., van Steeg, P., Meys, P., 2015. Wave runup and wave overtopping measurements using a laser scanner. Coast. Eng. 106, 20–29.

Hubbard, M.E., Dodd, N., 2002. A 2D numerical model of wave run-up and overtopping. Coast. Eng. 47, 1–26.

Hughes, S., Nadal, N., 2009. Laboratory study of combined wave overtopping and storm surge overflow of a levee. Coast. Eng. 56, 244–259.

Hughes, S.A., Thornton, C.I., 2016. Estimation of time-varying discharge and cumulative volume in individual overtopping waves. Coast. Eng. 117, 191–204.

Hunt, A., 2003. Extreme Waves, Overtopping and Flooding at Sea Defences. D.Phil. Thesis. University of Oxford.

Hunt-Raby, A.C., Borthwick, A.G., Stansby, P.K., Taylor, P.H., 2011. Experimental measurement of focused wave group and solitary wave overtopping. J. Hydraul. Res. 49, 450–464.

Ingram, D., Gao, F., Causon, D., Mingham, C., Troch, P., 2009. Numerical investigations of wave overtopping at coastal structures. Coast. Eng. 56, 190–202 The CLASH Project.

Jacobsen, N.G., van Gent, M.R., Wolters, G., 2015. Numerical analysis of the interaction of irregular waves with two dimensional permeable coastal structures. Coast. Eng. 102, 13–29.

Jonathan, P., Taylor, P.H., 1997. On irregular, nonlinear waves in a spread sea. J. Offshore Mech. Arctic Eng. 119, 37–41. https://doi.org/10.1115/1.2829043.

Li, T., Troch, P., Rouck, J.D., 2004. Wave overtopping over a sea dike. J. Comput. Phys. 198, 686–726.

Liang, Q., Borthwick, A.G., 2009. Adaptive quadtree simulation of shallow flows with wet-dry fronts over complex topography. Comput. Fluids 38, 221–234.

Lindgren, G., 1970. Some properties of a normal process near a local maximum. Ann. Math. Stat. 41, 1870–1883.

Losada, I.J., Lara, J.L., Guanche, R., Gonzalez-Ondina, J.M., 2008. Numerical analysis of wave overtopping of rubble mound breakwaters. Coast. Eng. 55, 47–62.

Lykke Andersen, T., Burcharth, H., 2009. Three-dimensional investigations of wave overtopping on rubble mound structures. Coast. Eng. 56, 180–189.

Madsen, P.A., Sørensen, O.R., 1992. A new form of the Boussinesq equations with improved linear dispersion characteristics. (Part 2). Coast. Eng. 18, 183–204.

Madsen, P.A., Murray, R., Sørensen, O.R., 1991. A new form of the Boussinesq equations with improved linear dispersion characteristics (Part 1). Coast. Eng. 15, 371–388.

McCabe, M., Stansby, P., Apsley, D., 2013. Random wave runup and overtopping a steep sea wall: shallow-water and boussinesq modelling with generalised breaking and wall impact algorithms validated against laboratory and field measurements. Coast. Eng. 74, 33–49.

Molines, J., Medina, J.R., 2015. Calibration of overtopping roughness factors for concrete armor units in non-breaking conditions using the CLASH database. Coast. Eng. 96, 62–70.

Neelamani, S., SchÃ¼ttrumpf, H., Muttray, M., Oumeraci, H., 1999. Prediction of wave pressures on smooth impermeable seawalls. Ocean Eng. 26, 739–765.

Orszaghova, J., 2011. Solitary Waves and Wave Groups at the Shore. D.Phil. Thesis. University of Oxford.

Orszaghova, J., Borthwick, A.G., Taylor, P.H., 2012. From the paddle to the beach - a Boussinesq shallow water numerical wave tank based on Madsen and Sørensen's equations. J. Comput. Phys. 231, 328–344.

Orszaghova, J., Taylor, P.H., Borthwick, A.G., Raby, A.C., 2014. Importance of second-order wave generation for focused wave group run-up and overtopping. Coast. Eng. 94, 63–79.

Oumeraci, H., Klammer, P., Partenscky, H.W., 1993. Classification of breaking wave loads on vertical structures. J. Waterw. Port, Coast. Ocean Eng. 119, 381–397.

Oumeraci, H., Kortenhaus, A., Allsop, W., de Groot, M., Crouch, R., Vrijling, H., Voortman, H., 2001. Probabilistic Design Tools for Vertical Breakwaters. CRC Press.

Owen, M., 1982. The hydraulic design of sea-wall profiles. In: Proceedings ICE on Shoreline Protection. Institution of Civil Engineers. Thomas Telford, pp. 185–192.

Pillai, K., Etemad-Shahidi, A., Lemckert, C., 2017. Wave overtopping at berm breakwaters: review and sensitivity analysis of prediction models. Coast. Eng. 120, 1–21.

Pullen, T., Allsop, N.W.H., Bruce, T., Kortenhaus, A., Schüttrumpf, H., van der Meer, J.W., 2007. EurOtop Wave Overtopping of Sea Defenses and Related Structures - Assessment Manual.

Pullen, T., Allsop, W., Bruce, T., Pearson, J., 2009. Field and laboratory measurements of mean overtopping discharges and spatial distributions at vertical seawalls. Coast. Eng. 56, 121–140 The CLASH Project.

Reeve, D., Soliman, A., Lin, P., 2008. Numerical study of combined overflow and wave overtopping over a smooth impermeable seawall. Coast. Eng. 55, 155–166.

Romano, A., Bellotti, G., Briganti, R., Franco, L., 2015. Uncertainties in the physical modelling of the wave overtopping over a rubble mound breakwater: the role of the seeding number and of the test duration. Coast. Eng. 103, 15–21.

Santo, H., Taylor, P.H., Eatock Taylor, R., Choo, Y.S., 2013. Average properties of the largest waves in Hurricane Camille. J. Offshore Mech. Arctic Eng. 135, 1–7.

Schäffer, H.A., 1996. Second-order wavemaker theory for irregular waves. Ocean Eng. 23, 47–88.

Schløer, S., Bredmose, H., Ghadirian, A., 2017. Analysis of experimental data: the average shape of extreme wave forces on monopile foundations and the newforce model. Energy Proc. 137, 223–237.

Suzuki, T., Altomare, C., Veale, W., Verwaest, T., Trouw, K., Troch, P., Zijlema, M., 2017. Efficient and robust wave overtopping estimation for impermeable coastal structures in shallow foreshores using SWASH. Coast. Eng. 122, 108–123.

Taylor, P.H., Williams, B.A., 2004. Wave statistics for intermediate depth water - NewWaves and symmetry. J. Offshore Mech. Arctic Eng. 126, 54–59. https://doi.org/10.1115/1.1641796.

Tofany, N., Ahmad, M., Mamat, M., Mohd-Lokman, H., 2016. The effects of wave activity on overtopping and scouring on a vertical breakwater. Ocean Eng. 116, 295–311.

Tonelli, M., Petti, M., 2013. Numerical simulation of wave overtopping at coastal dikes and low-crested structures by means of a shock-capturing boussinesq model. Coast. Eng. 79, 75–88.

Troch, P., Geeraerts, J., de Walle, B.V., Rouck, J.D., Damme, L.V., Allsop, W., Franco, L., 2004. Full-scale wave-overtopping measurements on the Zeebrugge rubble mound breakwater. Coast. Eng. 51, 609–628.

Tromans, P.S., Anaturk, A.R., Hagemeijer, P., 1991. A new model for the kinematics of large ocean waves - application as a design wave. In: Proceedings of the First International Offshore and Polar Engineering Conference. The International Society of Offshore and Polar Engineers, pp. 64–71.

Tuan, T.Q., Oumeraci, H., 2010. A numerical model of wave overtopping on seadikes. Coast. Eng. 57, 757–772.

van Damme, M., 2016. Distributions for wave overtopping parameters for stress strength analyses on floodembankments. Coast. Eng. 116, 195–206.

Van der Meer, J.W., 1998. Balkema, Rotterdam. Chapter Wave Run-up and Overtopping.

van der Meer, J., Tfnjes, P., de Waal, H., 1998. A code for dike height design and examination. In: Proceedings International Conference on Coastlines, Structures and Breakwaters. Institution of Civil Engineers. Thomas Telford, pp. 5–19.

van der Meer, J.W., Verhaeghe, H., Steendam, G.J., 2009. The new wave overtopping database for coastal structures. Coast. Eng. 56, 108–120 The CLASH Project.

van der Meer, J.W., Hardeman, B., Steendam, G.J., Schuttrumpf, H., Verheij, H., 2011. Flow depths and velocities at crest and landward slope of a dike, in theory and with the wave overtopping simulator. Coast. Eng. Proc. 1, 10.

Van der Meer, J., Allsop, W., H, N.W., Bruce, T., De Rouck, J., Kortenhaus, A., Pullen, T.H., Schüttrumpf, H., Troch, P., Zanuttigh, B., 2016. Manual on Wave Overtopping of Sea Defenses and Related Structures. An Overtopping Manual Largely Based on European Research, but for Worldwide Application.

Van Doorslaer, K., Romano, A., De Rouck, J., Kortenhaus, A., 2017. Impacts on a storm

wall caused by non-breaking waves overtopping a smooth dike slope. Coast. Eng. 120, 93–111.
van Gent, M.R., van den Boogaard, H.F., Pozueta, B., Medina, J.R., 2007. Neural network modelling of wave overtopping at coastal structures. Coast. Eng. 54, 586–593.
Vanneste, D., Troch, P., 2015. 2d numerical simulation of large-scale physical model tests of wave interaction with a rubble-mound breakwater. Coast. Eng. 103, 22–41.
Verhaeghe, H., De Rouck, J., van der Meer, J., 2008. Combined classifier–quantifier model: a 2-phases neural model for prediction of wave overtopping at coastal structures. Coast. Eng. 55, 357–374.
Whittaker, C., Raby, A.C., Fitzgerald, C., Taylor, P.H., 2016. The average shape of large waves in the coastal zone. Coast. Eng. 114, 253–264.
Whittaker, C., Fitzgerald, C., Raby, A., Taylor, P., Orszaghova, J., Borthwick, A., 2017. Optimisation of focused wave group runup on a plane beach. Coast. Eng. 121, 44–55.
Williams, H.E., Briganti, R., Pullen, T., 2014. The role of offshore boundary conditions in the uncertainty of numerical prediction of wave overtopping using non-linear shallow water equations. Coast. Eng. 89, 30–44.
Zanuttigh, B., Formentin, S.M., van der Meer, J.W., 2016. Prediction of extreme and tolerable wave overtopping discharges through an advanced neural network. Ocean Eng. 127, 7–22.